Journal of Materials Chemistry C

ROYAL SOCIETY OF CHEMISTRY

PAPER

View Article Online
View Journal

Cite this: DOI: 10.1039/d5tc01502b

Advancing thermoplasmonic sensing: gold nanobipyramids for enhanced light-to-heat conversion†

Andreea Campu,[ab] Ioana Andreea Brezestean,[cd] Septimiu-Cassian Tripon,[ef] Simion Astilean [ag] and Monica Focsan [ag]*

Thermoplasmonic detection is a newly emerging application in the rapidly growing and promising field of thermoplasmonics. Accordingly, herein, an in-depth evaluation of thermoplasmonic performances of gold nanobipyramids (AuBPs) dispersed in colloidal solutions and immobilized on a filter paper substrate was provided, which revealed their ability for efficient and sensitive thermoplasmonic detection of simple and complex molecules. Concretely, AuBPs in aqueous solution with optical responses in and out of resonance with the 808 nm laser line were synthesized and their intrinsic light-to-heat conversion performances were assessed, revealing photothermal efficiencies (η) up to 74%. Subsequently, colloidal AuBPs were functionalized with 4-mercaptobenzoic acid (4-MBA), which is a simple and small molecule. Consequently, η decreased by up to 4%. Furthermore, their immobilization on Whatman no. 1 filter paper through immersion resulted in the preservation of their optical properties and intrinsic thermoplasmonic activity. Thermoplasmonic detection capabilities of the plasmonic paper were tested using 4-MBA and thiol-polyethylene glycol-amine (a thermo-sensitive complex polymer). Following the functionalization of the plasmonic paper, its photothermal activity significantly decreased, causing an increase in the cooling time constant; thus, both 4-MBA and thiolated PEG were detected *via* thermoplasmonic detection. Moreover, a LOD of 0.19 nM and a LOQ of 0.58 nM were determined for 4-MBA, proving the high biosensing efficiency of the plasmonic paper. Hence, these results contribute to the consolidation of the versatile thermoplasmonic detection of both simple and complex interactions, being a stepping stone in the development of simple and efficient thermoplasmonic nanosensors.

Received 10th April 2025,
Accepted 7th July 2025

DOI: 10.1039/d5tc01502b

rsc.li/materials-c

1. Introduction

In the early 2000s, the first approaches to exploit the heat generated by gold nanoparticles for biomedical applications emerged,[1,2] becoming the foundation of the rapidly growing and promising field called thermoplasmonics.[3] Recent developments in thermoplasmonics have impacted a broad range of scientific activities and communities, extending its applications beyond its initial implementation for photothermal therapy,[4] drug and gene delivery[5] and photoacoustic imaging[6] in nanomedicine,[7] cell biology, photothermal and hot-electron chemistry,[8] solar light harvesting,[9] soft matter[10] and nanofluidics.[11] Considerable progress has been made by the scientific community in providing a better understanding of the thermoplasmonic mechanism; however certain challenges still remain when it comes to the influence of nanoscale photothermal processes on the photothermal effect.[12]

Thermoplasmonic effect emerges as a result of the resonant excitation of the surface plasmons, which induces a series of

[a] Nanobiophotonics and Laser Microspectroscopy Center, Interdisciplinary Research Institute on Bio-Nano-Sciences, Babes-Bolyai University, Treboniu Laurian No. 42, Cluj-Napoca 400271, Romania. E-mail: andreea.campu@ubbcluj.ro, monica.iosin@ubbcluj.ro
[b] Research Center for Complex Physical Systems, Faculty of Sciences, Lucian Blaga University, Doctor Ion Rațiu No. 5-7, Sibiu 550012, Romania
[c] Department of Molecular and Biomolecular Physics, National Institute for Research and Development of Isotopic and Molecular Technologies, Donat No. 67-103, Cluj-Napoca 400293, Romania. E-mail: ioana.brezestean@itim-cj.ro
[d] RDI Laboratory of Applied Raman Spectroscopy, RDI Institute of Applied Natural Sciences (IRDI-ANS), Babes-Bolyai University, Fântânele No. 42, Cluj-Napoca 400293, Romania
[e] Electron Microscopy Center "Prof. C. Craciun", Babes-Bolyai University, Clinicilor No. 5-7, Cluj-Napoca 400006, Romania. E-mail: septimiu.tripon@itim-cj.ro
[f] Electron Microscopy Integrated Laboratory, National Institute for Research and Development of Isotopic and Molecular Technologies, Donat No. 67-103, Cluj-Napoca 400293, Romania
[g] Biomolecular Physics Department, Faculty of Physics, Babes-Bolyai University, Mihail Kogalniceanu No. 1, Cluj-Napoca 400084, Romania. E-mail: simion.astilean@ubbcluj.ro

† Electronic supplementary information (ESI) available. See DOI: https://doi.org/10.1039/d5tc01502b

waterfall phenomena because of the energy transfer from the photons to the localized surface electrons and ultimately to the surrounding environment in the form of heat.[13] Upon the plasmon-induced resonance energy transfer, radiative and non-radiative damping processes take place, followed by the generation of hot carriers that transfer the energy to the material lattice upon their relaxation. The material lattice ultimately dissipates this energy to the surrounding environment as heat, through conduction, convection or radiation, either by localized or collective heating mechanisms. Consequently, thermal-induced processes such as mass transport, phase transitions, or chemical reactions can be induced.[3] The thermoplasmonic effect is highly dependent on the light absorption capability of plasmonic materials, which is considered a detrimental factor in the photothermal performances.[14] In this context, metallic nanoparticles are remarkably attractive owing to their increased energy absorption capacity at plasmon wavelengths.[9] In particular, gold nanoparticles have shown great potentials to operate as localized heat nanosources owing to their localized surface plasmon resonance (LSPR); the oscillations of the localized surface conduction electrons, resulting from the interactions with incoming light, produce a considerable temperature increase. Consequently, gold nanoparticles have been extensively implemented as thermoplasmonic generators in the development of alternative cancer treatments – photothermal therapy,[15–17] antibacterial activity[18,19] as well as, more recently, detection of viral sequences.[20] In particular, gold bipyramids (AuBPs) are good candidates for developing nanosystems as therapeutic agents for photothermal therapy.[21,22] Recently, their use as thermoplasmonic nanogenerators has contributed significantly to the development of the emerging application of thermoplasmonic detection. AuBPs-based photothermal sensors have been successful in evaluating antioxidant capacity by detecting ascorbic acid up to 0.08 μM,[23] developing photothermal immunoassays capable of detecting toxins up to 0.20 ng mL^{-1},[24] realizing thermoplasmonic detection of cardiac biomarkers up to 4.2 pg mL^{-1} [25] and as nanoreactors for bioassays with dynamic detection range from 5 ng μL^{-1} to 1 pg μL^{-1}.[26] However, in these studies, the measured signals originated from photothermally induced reactions or modifications in the environment of the nanoparticles.

Therefore, in this work, in order to gain better insights on the photothermal mechanism, we exploited the intrinsic capabilities of AuBPs to efficiently convert light to heat for realizing thermoplasmonic detection, both in solution and when immobilized on a flexible filter paper, consolidating the detection method and developing sensitive thermoplasmonic sensors. We evaluated the photothermal conversion performances of colloidal nanoparticles by determining their photothermal efficiencies. By functionalizing the AuBPs with a small molecule (4-mercaptobenzoic acid (4-MBA)), variations in their light-to-heat conversion were monitored. AuBPs with their longitudinal LSPR at 811 nm exhibited the best photothermal features and thermoplasmonic detection abilities; therefore, they were further immobilized on a Whatman paper. The photothermal performance of the plasmonic paper was evaluated and optimized by increasing the immobilized AuBPs concentration. The thermoplasmonic detection capabilities of the optimized, flexible plasmonic-paper-based nanoplatform were verified using two target analytes–4-MBA as a small, simple molecule and thiol-polyethylene glycol-amine as a thermo-sensitive complex polymer. The mass effect and thermally induced phase transition led to modifications in the photothermal conversion performances and, implicitly, cooling time constants of the plasmonic paper. Thus, AuBPs, both in solution and immobilized on a paper substrate, were demonstrated to operate as efficient thermoplasmonic sensors that enable the detection of simple and complex molecules, contributing to a comprehensive understanding of the versatile thermoplasmonic detection technique.

2. Experimental section

2.1. Materials

Tetrachloroauric acid ($HAuCl_4 \cdot 4H_2O$, 99.99%), cetyltrimethylammonium bromide (CTAB, 96%), nitric acid (HNO_3, 65%), citric acid ($C_6H_8O_7$), cetyltrimethylammonium chloride (CTAC), hydroxyquinoline (HQL, 99%), sodium borohydride ($NaBH_4$, 99%), silver nitrate ($AgNO_3$, 99%), 4-mercaptobenzoic acid (4-MBA), thiol-polyethylene glycol-amine (SH-PEG-NH_2, average M_w of 3500 Da) and Whatman qualitative filter paper grade 1 were purchased from Sigma-Aldrich. All chemicals were used as received. Ultra-pure water with a resistivity of ~18.2 MΩ was used as the solvent throughout the experiments.

2.2. Functionalization of the colloidal AuBPs and flexible plasmonic-paper-based nanoplatform

To evaluate the potential of the colloidal AuBPs to operate as transducers for thermoplasmonic detection, 4-mercaptobenzoic acid – as a small simple molecule, was selected. An ethanoic solution of 10^{-3} M of 4-MBA was prepared and mixed with AuBPs in a volume ratio of 1 : 9, thus obtaining a final 4-MBA concentration of 10^{-4} M.

For evaluating the thermoplasmonic detection ability of the plasmonic paper, both 4-MBA and thiol-polyethylene glycol-amine – a thermo-sensitive, complex polymer with a molecular weight of 3500 Da, were tested. Specifically, 10 μL of the 4-MBA ethanoic 10^{-4} M solution was added dropwise onto the plasmonic paper and allowed to dry. SH-PEG-NH_2 was prepared in ultra-pure water at a concentration of 0.25 mM, and 10 μL of the thiolated PEG was added dropwise onto the plasmonic paper and allowed to dry under room temperature conditions. To determine the detection limit, 10 μL of ethanoic 4-MBA solutions with concentrations ranging from 10^{-4} to 10^{-10} M were dropped onto the plasmonic paper and allowed to dry at room temperature.

2.3. Thermographic determinations

Photothermal properties of the colloidal AuBPs aqueous solutions and plasmonic paper were determined based on thermographic determinations. To achieve this, the samples were irradiated from above using a Therapy Laser DTL–BCD–01 with an NIR excitation

wavelength of 808 nm. Using an Optris PI 450 infrared camera, thermographic images were recorded during and after laser exposure at a 45° angle (Fig. S5). Colloidal AuBPs (500 μL) were exposed to laser excitation for 10 minutes, followed by the monitoring of the cooling process for another 10 minutes; thermal images were recorded in real time every 30 seconds. As for the plasmonic paper samples, the exposure and cooling times were decreased to 5 minutes with the laser on and 5 minutes with the laser off, respectively, while thermal images were recorded in real time every 5 seconds. To study the dependency of the photothermal performance on the laser power, the plasmonic paper obtained after 5 successive immersions was exposed to the 808 nm laser line with varied laser powers, specifically 184, 232, 290 and 320 mW. For the determination of the detection limit, the exposure time was optimized as 3 minutes with the laser on and 3 minutes with the laser off. All the thermal experiments were realized in a dark room to avoid external contributions and conducted in triplicate to ensure reproducibility. The presented thermal curves were obtained as the average of the triplicates, and the standard deviation (SD) and standard error (SE) were calculated.

2.4. Characterization methods

The extinction spectra of the colloidal AuBPs in aqueous solution were recorded using a Jasco V-670 UV-Vis-NIR spectrophotometer with a 2 nm bandwidth and 1 nm spectral resolution. To record the LSPR spectra of the plasmonic paper samples, a portable Ocean Optics USB 4000 optical UV-Vis spectrophotometer was employed coupled with an inverted optical microscope ZEISS Axio Observer Z1 system equipped with a halogen lamp (HAL 100). The extinction spectra were recorded using a 20× ZEISS objective and an optical fibre with a 600 μm core diameter.

Thermoplasmonic determinations were realized in a dark room using a Therapy Laser DTL-BCD-01 equipped with a laser probe SL1 having an 808 nm diode. The measurements were realized with a laser power of 0.29 W. To record the thermographic images, an Optris PI 450 infrared camera with an O38 standard lens was used. The as-recorded thermal maps were analysed using the software of the camera, Optris PI Connect.

3. Results and discussion

3.1. Thermoplasmonic detection capabilities of colloidal AuBPs

Gold nanoparticles of different shapes and sizes have been previously studied as photothermal agents considering their application in photothermal therapy.[27–29] With the advancements in the emerging field of thermoplasmonic detection, their applicability has widened owing to their unique optical properties and intrinsic photothermal features. Accordingly, colloidal AuBPs in aqueous solutions were chemically synthesized to exhibit longitudinal LSPR responses in and out of resonance using an 808 nm laser line excitation, with the longitudinal LSPR specifically located at 693, 774 and 811 nm. The seed-mediated synthesis approach used to grow AuBPs along with their optical and morphological characterisations are described in the ESI.†

To assess the thermoplasmonic detection capabilities of the colloidal AuBPs in aqueous solutions, the light-to-heat conversion performances of the bipyramidal nanoparticles were first evaluated. In particular, AuBPs samples were exposed to the 808 nm laser excitation for 10 minutes, and then, the cooling process was monitored for another 10 minutes. During the heating and cooling of the nanoparticles, thermal images were recorded every 30 seconds. Fig. 1A presents representative thermographic maps recorded at 0, 2, 5, 7 and 10 minutes for the solvent (as control) and the three AuBPs samples. Notably, all the AuBPs samples exhibited photothermal conversion performances, reaching a maximum temperature of up to 49 °C for the AuBPs with longitudinal LSPR under resonance conditions with the 808 nm laser line excitation. The solvent (ultra-pure water) used as control did not show any light-to-heat conversion abilities.

To assess the light-to-heat conversion performances, the experimentally obtained thermographic images were analysed by extracting the temperatures (T) at every 30 seconds during the heating and cooling processes. Next, the temperature difference (ΔT) at respective times was calculated as the difference between the time-corresponding T and environmental temperature (T_{env}) as follows:

$$\Delta T = T - T_{env} \quad (1)$$

ΔT was then plotted against irradiation and cooling times to obtain the corresponding thermal curves (Fig. 1B). Thermal curves further validated the observations from thermal mappings. Additionally, the thermal determinations show that as the LSPR band is further away from the resonance condition with the excitation wavelength, the photothermal performances decrease. This can be attributed to the fact that the photothermal effect is highly dependent on the absorbance capabilities of the nanoparticles at the irradiation wavelength.[30] As the AuBPs with an LSPR in the out-of-resonance condition were able to absorb less energy at 808 nm, their ability to convert light to heat was reduced. After irradiation, the stability of the AuBPs was investigated by recording their extinction spectra and comparing it with the optical response recorded prior to laser excitation. As shown in Fig. 1C, the optical responses almost perfectly overlapped, demonstrating the high thermal stability of the nanobipyramidally shaped Au nanoparticles throughout the thermal experiments.

Moreover, the photothermal conversion efficiencies (η) were calculated using a previously reported analytical method relying on microscale thermal dynamics in solution, specifically, on the derivation of the energy balance that is used to fit the thermal data.[30] Thus, η was defined as:

$$\eta = \frac{h \times A\Delta T - I\zeta}{I(1-\zeta)(1-10^{-A_\lambda})} \quad (2)$$

where h is the heat transfer coefficient for AuBPs, A is the irradiation area cross section, I is the incident laser power,

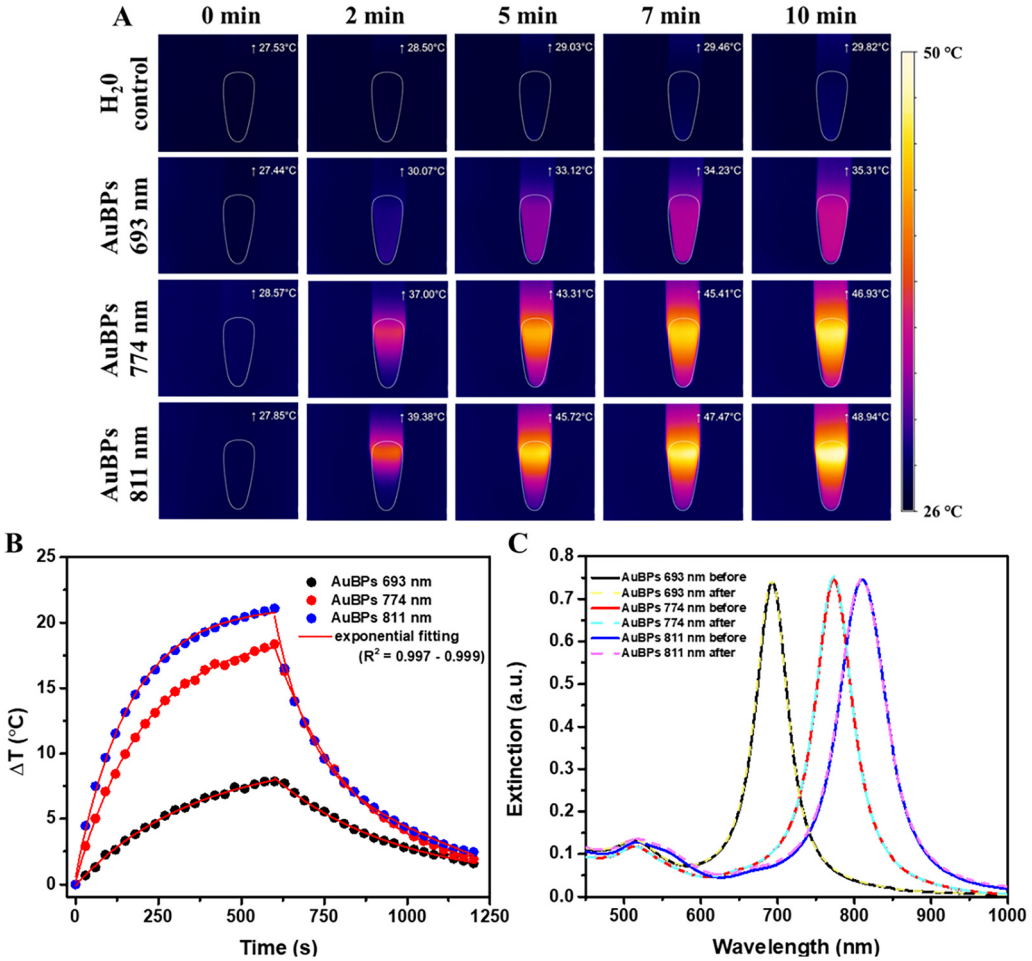

Fig. 1 (A) Representative thermographic images recorded during the irradiation of the colloidal AuBPs samples and ultra-pure water as the control sample, (B) thermal curves obtained from the temperatures extracted from the thermographic images and (C) UV-Vis-NIR extinction spectra recorded before (full lines) and after (dashed lines) exposure to the 808 nm laser for all AuBPs samples, indicating their high thermal stability.

ζ is the energy fraction absorbed by the Eppendorf tube and solvent (in this case, water), and A_λ is the absorbance of AuBPs at the 808 nm excitation wavelength.

As predicted, the calculated η values increased as the position of the longitudinal LSPR band approached resonance condition with the excitation laser wavelength (Table 1). Thus, η values of up to 74% were obtained for AuBPs with an LSPR of 811 nm.

Furthermore, the thermoplasmonic detection capabilities of AuBPs were evaluated. For this purpose, 4-mercaptobenzoic acid (4-MBA) molecule was chosen owing to its thiol active group, which is known to bind to the surface of gold.[31] First, we functionalized AuBPs with 4-MBA. To verify the success of functionalization, extinction spectra of the AuBPs were recorded after their exposure to 4-MBA, and the optical response were compared with those of the as-synthesized nanoparticles. The successful functionalization with 4-MBA was confirmed by the red-shifts of 1, 3 and 4 nm recorded for the longitudinal LSPR at 693, 774 and 811 nm, respectively (Fig. 2). LSPR is known to be highly sensitive to changes in the micro-environment in the close vicinity of the nanoparticles; hence, when 4-MBA was grafted on the surface of the nanoparticles, the refractive index at their surface got modified, resulting in a red-shift in the optical response. As the electromagnetic field is highly enhanced at the tips of the AuBPs,[32] their sensitivity to environmental changes is high at the tips, and therefore, only the longitudinal LSPR band was red-shifted.

Table 1 Maximum temperature differences with respect to the environmental temperature (ΔT_{max}) reached during irradiation, cooling time constant (τ_S) and calculated photothermal conversion efficiencies (η) before and after the functionalization of all the AuBPs colloidal solutions with 4-MBA

Sample	ΔT_{max} (°C)	τ_S (s)	η (%)
AuBPs 693 nm	8 ± 1	376.88	14
AuBPs 693 nm-MBA	7 ± 1	304.51	13
AuBPs 774 nm	18 ± 1	260.45	61
AuBPs 774 nm-MBA	20 ± 1	269.30	59
AuBPs 811 nm	21 ± 1	252.35	74
AuBPs 811 nm-MBA	22 ± 1	259.33	71

Subsequent to the functionalization of AuBPs with 4-MBA, the samples were exposed to the 808 nm laser under the same

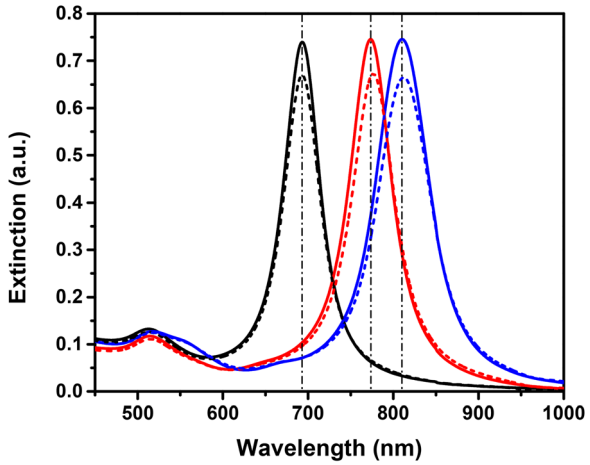

Fig. 2 UV-Vis-NIR extinction spectra recorded before (full lines) and after (dashed lines) the functionalization of AuBPs with 4-MBA.

conditions used for the as-synthesized nanoparticles. Based on the thermographic images, the thermal curves were plotted, and the photothermal efficiencies were calculated considering the mass addition of the 4-MBA. As shown in Table 1, the grafting of 4-MBA did not considerably affect the maximum temperature compared with the as-synthesized nanoparticles, indicating that the target analyte binding may have affected the intrinsic heat transfer rate of the surface oscillating electrons. However, the effect of target analyte binding was observed in photothermal conversion efficiencies: functionalization of AuBPs with 4-MBA resulted in decreased photothermal conversion efficiencies. The addition of the target analyte induced a change in the cooling process of AuBPs *via* a change in the cooling time constant. Thus, η was reduced by 7%, 3% and 4% (Table 1) for the AuBPs with longitudinal LSPR responses of 693, 774 and 811 nm, respectively.

Therefore, all AuBPs samples could operate as thermoplasmonic nanogenerators for thermoplasmonic detection applications with different performances, which are related to their absorbance characteristics. AuBPs with a longitudinal LSPR at 811 nm exhibited the best photothermal features and thermoplasmonic detection abilities; therefore, they were selected to subsequently develop flexible plasmonic-paper-based nanoplatforms.

3.2. Light-to-heat conversion performances of the plasmonic paper samples

The plasmonic paper was exposed to the 808 nm laser excitation in a dark room to avoid external contributions, similar to the solution-based systems. To determine the influence of the concentration of immobilized AuBPs, filter paper immersed once, thrice and five times, respectively, were investigated. Free filter paper was tested as the control. A thermographic image was captured every 5 seconds throughout the process involving 5 minutes of exposure and 5 minutes of cooling. The characteristic thermographic images recorded at 0, 1, 2 and 3 minutes are presented in Fig. 3A. All the samples exhibited photothermal

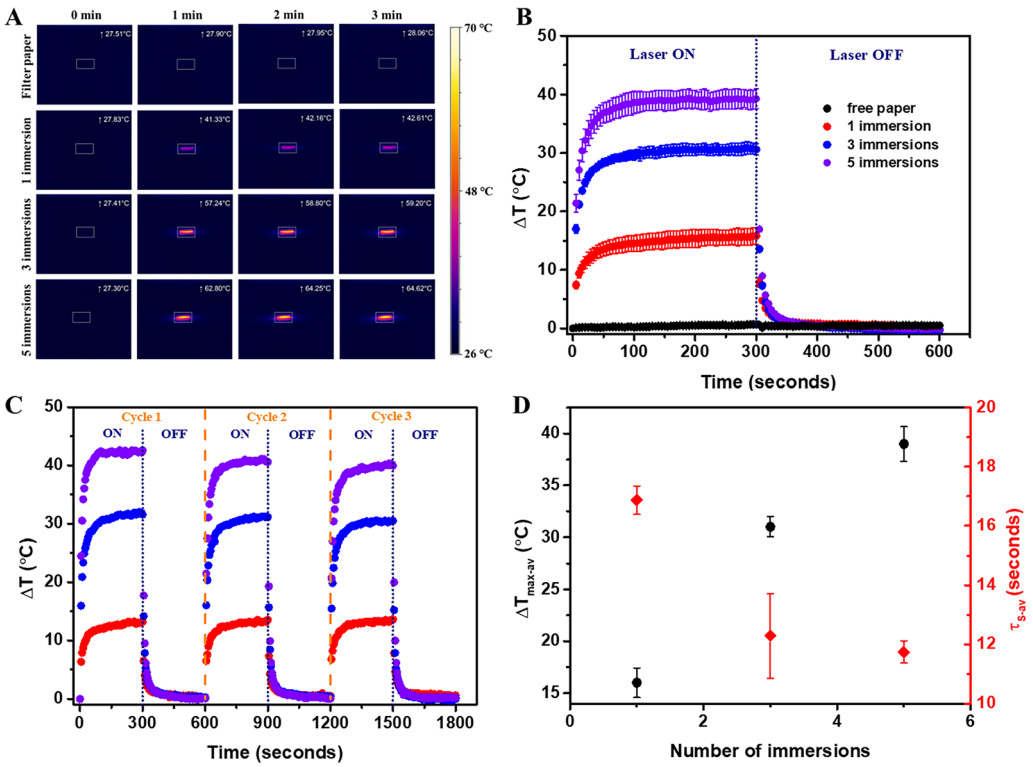

Fig. 3 (A) Thermographic images recorded during the laser exposure and (B) corresponding thermal curves of the free filter paper and plasmonic papers obtained after 1, 3 and 5 immersions. (C) Thermal curves obtained through three successive laser ON/OFF cycles, proving the high reusability of the plasmonic paper. (D) Plots of the average ΔT_{max} and τ_S with respect to the number of immersions.

activity, excluding the free filter paper, and thermal equilibrium was reached in the first 50 seconds following laser exposure. The temperatures were extracted from the thermographic images, and an average ΔT_{max} of 1 °C (SD 0.41, SE 0.24) was determined for the free filter paper, while the plasmonic papers obtained after 1, 3, and 5 immersions of the filter paper reached an average ΔT_{max} of 16 °C (SD 2.45, SE 1.41), 31 °C (SD 1.70, SE 0.98) and 39 °C (SD 2.89, SE 1.67), respectively. As expected, the thermal curves (Fig. 3B) confirmed that a higher immobilized AuBPs concentration led to improved photothermal conversion performances. Therefore, it was demonstrated that after the immobilization of the AuBPs onto the cellulose fibres, both the optical features and the intrinsic light-to-heat conversion properties of the colloidal AuBPs were preserved. Furthermore, the reusability of the plasmonic paper was tested by exposing it to a series of three consecutive laser ON/OFF cycles. As shown in Fig. 3C, all plasmonic papers showed negligible variations in terms of temperature increase, thus exhibiting excellent thermal stability and indicating the possibility of performing multiple measurements on the same platform without altering its photothermal conversion capability. Moreover, the photothermal performances of the plasmonic paper samples were analyzed as a function of the cooling time constant (τ_S), which was extracted as the slope of the linear regression of the cooling profile obtained by plotting the cooling time against the negative normal logarithm of the temperature driving force (θ), which is calculated as:

$$\theta = \frac{T - T_{env}}{T_{max} - T_{env}} \quad (3)$$

where T_{max} corresponds to the maximum temperature recorded during the laser exposure. It was found that as the AuBPs concentration increased, τ_S decreased. For the free filter paper, a τ_S of 41 s was calculated, whereas for the plasmonic papers, τ_S of 37.05, 32.59 and 32.25 s were obtained for one, three and five immersions, respectively. Thus, as the plasmonic paper exhibited similar thermal performances, their cooling process also followed a similar pattern, as can be seen from the close values of the cooling time constant. Subsequently, for thermoplasmonic detection experiments, the plasmonic paper obtained after 5 successive immersions was used as it offered the best thermoplasmonic performance.

Furthermore, the plasmonic paper with the best performance was exposed to different laser powers (184, 232, 290 and 320 mW), and thermographic images were recorded every 5 seconds for 5 minutes with the laser on and 5 minutes with the laser off. Fig. 4A shows the average thermal curves obtained from the extraction of the temperatures from the triplicate measurements and the determination of the average ΔT. At a laser power of 184 mW, an average ΔT_{max} of 23 °C was obtained with an SD of 2.19 and an SE of 1.26; at a 232 mW laser power, an average ΔT_{max} of 36 °C was obtained with an SD of 2.25 and an SE of 1.30; at a 290 mW laser power, an average ΔT_{max} of 39 °C was obtained with an SD of 2.99 and an SE of 1.73; and at a 320 mW laser power, an average ΔT_{max} of 47 °C was obtained with an SD of 2.5 and an SE of 1.44. These results demonstrated that increasing the laser power improved the light-to-heat conversion performance. The plot of the average ΔT_{max} against the laser power (Fig. 4B) showed a linear dependency between the photothermal performance and the power of the irradiation source.

3.3. Thermoplasmonic detection abilities of the flexible plasmonic-paper-based nanoplatform

In order to evaluate the thermoplasmonic detection capabilities of the flexible plasmonic-paper-based nanoplatform, two molecules were tested: 4-MBA – a small molecule and SH-PEG-NH_2 – a linear, heterobifunctional thermo-sensitive polymer with a molecular weight of 3500 Da, as a complex molecule. 4-MBA was used to verify if the thermoplasmonic performance relied on the same mechanism as in solution, specifically the modification of the intrinsic heat transfer rate of the surface oscillating electrons or it relied on the mass effect. Both molecules bound to the AuBPs through their thiol active groups. Extinction spectra were recorded before and after their functionalization (Fig. 5A). After the functionalization with 4-MBA 10^{-4} M, the longitudinal LSPR of the immobilized AuBPs was red-shifted by 7 nm (Fig. 5A-red spectrum), while a 16 nm

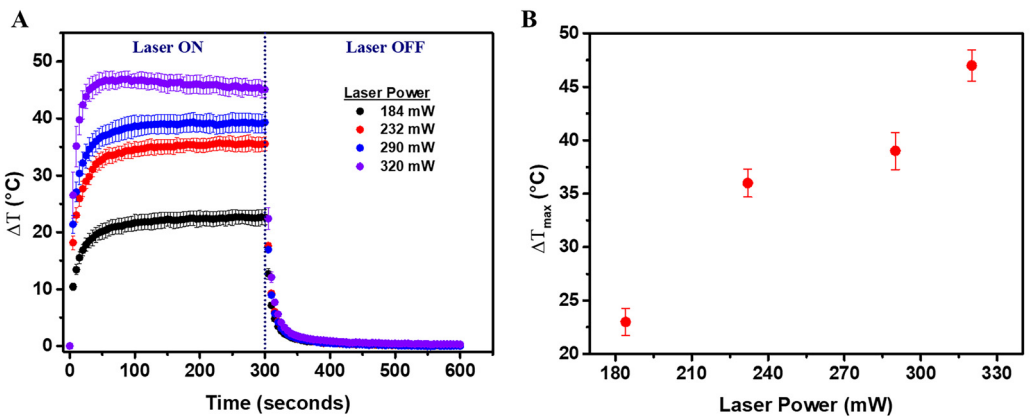

Fig. 4 (A) Average thermal curves obtained for the tested laser powers (184, 232, 290 and 320 mW). (B) Plot of the maximum temperature reached as a function of the employed laser power.

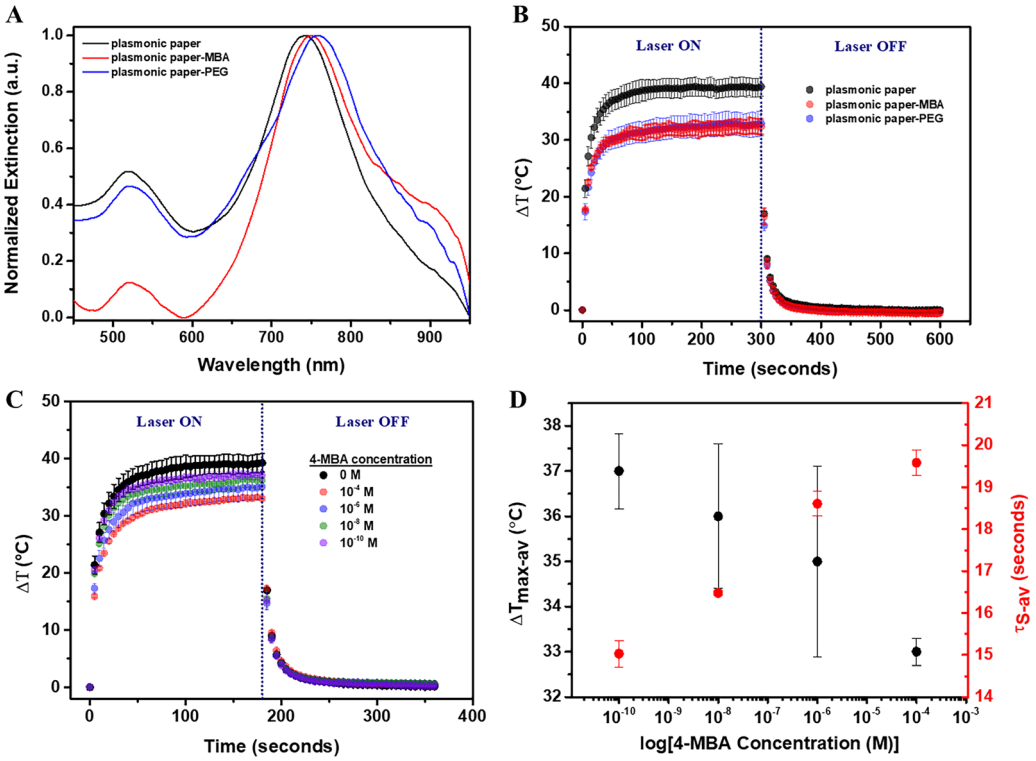

Fig. 5 (A) Extinction spectra recorded before and after grafting 4-MBA 10^{-4} M and SH-PEG-NH_2 onto the surface of the immobilized AuBPs. (B) Average thermal curves obtained from the thermographic images recorded during the exposure of the functionalized plasmonic papers to an 808 nm laser wavelength. (C) Average thermal curves obtained from the thermographic images recorded during the exposure of the plasmonic papers at an 808 nm laser wavelength after being functionalized with 4-MBA ethanoic solutions at different concentrations (10^{-4}, 10^{-6}, 10^{-8} and 10^{-10} M). (D) Plots of the average ΔT_{max} and τ_S values with respect to the logarithm of the 4-MBA concentrations.

red-shift was induced by the attachment of the SH-PEG-NH2 (Fig. 5A-blue spectrum), confirming the successful functionalization of the plasmonic paper with both 4-MBA (denoted as plasmonic paper-MBA) and SH-PEG-NH_2 (denoted as plasmonic paper-PEG).

Subsequently, the plasmonic paper-MBA and plasmonic paper-PEG were exposed to the 808 nm laser excitation for 5 minutes, and thermographic monitoring was maintained for another 5 minutes to allow the samples to cool to the environmental temperature. Fig. 5B shows the thermal curves obtained from the analysis of the thermographic images. Initially, the functionalization with 4-MBA 10^{-4} M resulted in a substantial decrease in the photothermal activity, and ΔT was 5 °C lower than that of the unfunctionalized plasmonic paper. This decrease in the light-to-heat conversion performance was confirmed by the increase of τ_S from 11.74 to 19.58 s (SD 0.54, SE 0.31). In this case, the decrease in photothermal efficiency resulted from the effect of mass addition. Furthermore, compared with the plasmonic paper, the heating process was rather slower as the plasmonic paper reached thermal equilibrium at around 60 seconds of laser exposure, while the plasmonic paper-MBA required several more seconds to equilibrate. The thermal curve of the plasmonic paper-PEG showed a similar behavior as the recorded temperature reached 33 °C. Experimentally, the temperature recorded using the thermographic camera represented the maximum temperature recorded on a specific, user-defined area. Therefore, it is assumed that the local temperature reached at the nanoparticle level is much higher. In the case of the plasmonic paper-PEG, the polymer suffered a phase change leading to a τ_S of 11.79 s (SD 2.48, SE 1.43) after 60 seconds of laser exposure, which is comparable with the cooling time constant of the plasmonic paper. It has been reported in literature that PEG is highly stable as a bulk material at freezing temperatures, while it gradually degrades in air or as a solute. Depending on its molecular weight, its melting point varies from 5 to 62 °C;[33] therefore, relatively low temperatures can result in a phase transfer. Furthermore, the limits of detection (LOD) and quantification (LOQ) of the plasmonic paper were evaluated. Notably, the plasmonic paper was functionalized with 4-MBA ethanoic solutions of concentrations ranging between 10^{-4} to 10^{-10} M. The functionalized plasmonic papers were then exposed to an 808 nm laser line for 3 minutes followed by 3 minutes of cooling. Based on the thermographic images recorded in triplicate, average thermal curves were obtained (Fig. 5C), demonstrating that the mass addition decreased the light-to-heat conversion performance. As the 4-MBA concentration decreased, the average ΔT_{max} increased towards the ΔT_{max} of the unfunctionalized plasmonic paper. As shown in Fig. 5D, the SE in for ΔT_{max} was rather high and did not permit an accurate detection. Therefore, τ_S, which is highly sensitive to the addition of mass, was extracted from the cooling process. Fig. 5D presents

the dependency of the determined average τ_S to the logarithmic value of the 4-MBA concentration. A high concentration of 4-MBA increased the average τ_S to 19.58 s (SD 0.52, SE 0.31) for 4-MBA 10^{-4} M. With decreasing concentration, the average τ_S decreased, resulting in the values of 18.61 s (SD 0.5, SE 0.29) for 4-MBA 10^{-6} M, 16.48 s (SD 0.11, SE 0.06) for 4-MBA 10^{-8} M, and 15.03 s (SD 0.54, SE 0.31) for 4-MBA 10^{-10} M, respectively. Moreover, an LOD of 0.19 nM and LOQ of 0.58 nM were calculated using the following equations:

$$\text{LOD} = 3.3 \times \frac{\text{standard deviation of the ordinate intercept}}{\text{slope of the regression line}} \quad (4)$$

$$\text{LOQ} = 10 \times \frac{\text{standard deviation of the ordinate intercept}}{\text{slope of the regression line}} \quad (5)$$

The proposed flexible plasmonic-paper-based nanoplatform exhibited enhanced thermoplasmonic detection capabilities for 4-MBA molecule compared with the performances of the corresponding colloidal nanoparticles. Although the colloidal AuBPs showed a 6% increase in the cooling time constant after the functionalization with 4-MBA, the plasmonic paper-MBA exhibited a 67% increase in τ_S. Furthermore, the nanomolar LOD and LOQ were determined, which demonstrated the ability of the plasmonic paper to be efficiently implemented in thermoplasmonic detection applications.

4. Conclusions

In summary, this work reported the intrinsic thermoplasmonic properties of colloidal gold nanobipyramids (AuBPs) and AuBPs-based paper nanoplatforms in order to provide an in-depth evaluation of their thermoplasmonic performances, which revealed their ability for the efficient and sensitive thermoplasmonic detection of simple and complex molecules. AuBPs with longitudinal LSPR responses located at 693, 774 and 811 nm were synthesized in an aqueous solution, and their intrinsic light-to-heat conversion performances were assessed upon their exposure to an 808 nm laser line, which realized photothermal efficiencies (η) of up to 64%. Their functionalization with 4-mercaptobenzoic acid (4-MBA) induced a decrease in η from 5% to 8%, suggesting a change in the intrinsic heat transfer rate of the oscillating electrons. Additionally, after their immobilization on Whatman no. 1 filter paper, their optical properties and intrinsic thermoplasmonic activity were preserved. The photothermal conversion performances were significantly decreased after the functionalization of the plasmonic paper with 4-MBA, which resulted in an increased cooling-time constant. The functionalization with thiol-polyethylene glycol-amine thermo-sensitive polymer also highlighted the light-to-heat conversion performances; however, the cooling time constant revealed no change, suggesting a phase transition of the polymer owing to high local temperatures. An LOD of 0.19 nM and an LOQ of 0.58 nM were determined for 4-MBA, proving the high biosensing efficiency of the plasmonic paper. Hence, these results contribute to the consolidation of the versatile thermoplasmonic detection of both simple and complex interactions, being a stepping stone in the development of simple and efficient thermoplasmonic nanosensors.

Author contributions

Andreea CAMPU: conceptualization, methodology, investigation, formal analysis, writing – original draft, review and editing, project administration, funding acquisition; Ioana Andreea Brezestean: investigation; Septimiu-Cassian Tripon: investigation; Simion ASTILEAN: writing – review and editing, Monica FOCSAN: writing – review and editing, project administration, funding acquisition.

Conflicts of interest

The authors declare no conflicts of interest.

Data availability

The data supporting this article have been included as part of the ESI.†

Acknowledgements

This work was supported by the Babes-Bolyai University through the Starting Research Grant (SRG-UBB), contract no. 32984/23.06.2023 and by the project ''Plasmon mediated biology: Exploitation of plasmonics to investigate and enhance biological processes and application to biomedical issues (acronym: BioPlasmonics)'' funded by European Union – NextgenerationEU and Romanian Government, under National Recovery and Resilience Plan for Romania, contract no 760037/23.05.2023, cod PNRR-C9-I8-CF-199/28.11.2022 through the Romanian Ministry of Research, Innovation and Digitalization, within Component 9, Investment I8. I. A. B. acknowledges the financial support from the Romanian Ministry of Research, Innovation and Digitalization through the ''Nucleu'' Programme within the National Plan for Research, Development and Innovation 2022–2027, project PN 23 24 01 02.

References

1 G. Huttmann and R. Birngruber, *IEEE J. Sel. Top. Quantum Electron.*, 1999, **5**, 954–962.
2 D. Boyer, P. Tamarat, A. Maali, B. Lounis and M. Orrit, *Science*, 2002, **297**, 1160–1163.
3 G. Baffou, *Thermoplasmonics: Heating Metal Nanoparticles Using Light*, Cambridge University Press, Cambridge, 2017.
4 L. R. Hirsch, R. J. Stafford, J. A. Bankson, S. R. Sershen, B. Rivera, R. E. Price, J. D. Hazle, N. J. Halas and J. L. West, *Proc. Natl. Acad. Sci. U. S. A.*, 2003, **100**, 13549–13554.
5 P. Ghosh, G. Han, M. De, C. Kim and V. Rotello, *Adv. Drug Delivery Rev.*, 2008, **60**, 1307–1315.
6 W. Li and X. Chen, *Nanomedical*, 2015, **10**, 299–320.

7 A. Guglielmelli, F. Pierini, N. Tabiryan, C. Umeton, T. J. Bunning and L. De Sio, *Adv. Photonics Res.*, 2021, **2**, 2000198.
8 Y. Zhao, L. Sang and Z. Ren, *Sol. Energy Mater. Sol. Cells*, 2024, **267**, 112728.
9 G. Liu, J. Xu, T. Chen and K. Wang, *Phys. Rep.*, 2022, **981**, 1–50.
10 A. Sepúlveda and D. Boudreau, *ACS Appl. Polym. Mater.*, 2024, **6**, 2359–2370.
11 S. Ezendam, L. Nan, I. L. Violi, S. A. Maier, E. Cortés, G. Baffou and J. Gargiulo, *Adv. Opt. Mater.*, 2024, **12**, 2301496.
12 G. Baffou, F. Cichos and R. Quidant, *Nat. Mater.*, 2020, **19**, 946–958.
13 B. Yang, C. Li, Z. Wang and Q. Dai, *Adv. Mater.*, 2022, **34**, 2107351.
14 Y. Li, W. Li, T. Han, X. Zheng, J. Li, B. Li, S. Fan and C.-W. Qiu, *Nat. Rev. Mater.*, 2021, **6**, 488–507.
15 N. S. Abadeer and C. J. Murphy, *J. Phys. Chem. C*, 2016, **120**, 4691–4716.
16 D. Khurana, A. K. Shaw, G. Sharma, M. Ahmed, S. K. Shukla and S. Soni, *Int. Commun. Heat Mass Transf.*, 2024, **156**, 107597.
17 M. Ghaffarlou, H. Rashidzadeh, A. Mohammadi, N. Mousazadeh, M. Barsbay, A. Sharafi, M. Gharbavi, H. Danafar and S. Javani, *Sci. Rep.*, 2024, **14**, 13299.
18 Y. Feng, Q. Sun, P. Liu, W. Fan and B. Fan, *Int. J. Nanomed.*, 2024, **19**, 6981–6997.
19 J. Lv, Y. Qiu, L. Pan, X. Zhang, M. Li and X. Yin, *Nano TransMed*, 2024, **3**, 100034.
20 G. Qiu, Z. Gai, Y. Tao, J. Schmitt, G. A. Kullak-Ublick and J. Wang, *ACS Nano*, 2020, **14**, 5268–5277.
21 X. Wu, L. Mu, M. Chen, S. Liang, Y. Wang, G. She and W. Shi, *ACS Appl. Bio Mater.*, 2019, **2**, 2668–2675.
22 M. Mohammadzadeh, S. Labbaf and A. Kermanpur, *Adv. Theory Simul.*, 2024, 2400005.
23 J. Huang, F. Jiang, Z. Zhao, Z. Li, X. Deng, R. P. S. Han, S. Xu, Y. Tao and Z. Lin, *ACS Appl. Nano Mater.*, 2024, **7**, 14621–14628.
24 Y. Wang, L. Ma, L. Xie, Q. Wu, Y. Liu, Q. Zhao, Y. Zhang, B. Jiao and Y. He, *ACS Appl. Nano Mater.*, 2023, **6**, 17858–17868.
25 A. Campu, I. Muresan, M. Potara, D. R. Lazar, F.-L. Lazar, S. Cainap, D. M. Olinic, D. Maniu, S. Astilean and M. Focsan, *J. Mater. Chem. B*, 2024, **12**, 962–972.
26 J.-H. Lee, Z. Cheglakov, J. Yi, T. M. Cronin, K. J. Gibson, B. Tian and Y. Weizmann, *J. Am. Chem. Soc.*, 2017, **139**, 8054–8057.
27 A. Campu, M. Focsan, F. Lerouge, R. Borlan, L. Tie, D. Rugina and S. Astilean, *Colloids Surf., B*, 2020, **194**, 111213.
28 B. J. Delgado-Corrales, V. Chopra and G. Chauhan, *J. Mater. Chem. B*, 2025, **13**, 399–428.
29 X. Zeng, L. Tang, W. Zhang, X. Hong and Y. Xiao, *Small*, 2025, 2412296.
30 A. Campu, A.-M. Craciun, M. Focsan and S. Astilean, *Nanotechnology*, 2019, **30**, 405701.
31 F. M. M. Aldosari, *Molecules*, 2022, **27**, 892.
32 A. Campu, F. Lerouge, D. Chateau, F. Chaput, P. Baldeck, S. Parola, D. Maniu, A. M. Craciun, A. Vulpoi, S. Astilean and M. Focsan, *Anal. Chem.*, 2018, **90**, 8567–8575.
33 R. Paberit, E. Rilby, J. Göhl, J. Swenson, Z. Refaa, P. Johansson and H. Jansson, *ACS Appl. Energy Mater.*, 2020, **3**, 10578–10589.